

# Tuning the Magnetic Anisotropy of $\text{La}_{2/3}\text{Sr}_{1/3}\text{MnO}_3$ by Controlling the Structure of $\text{SrCoO}_x$ in the Corresponding Bilayers Using Ionic-Liquid Gating

Jinghua Song,<sup>1,2</sup> Yuansha Chen,<sup>1,3,†</sup> Xiaobing Chen,<sup>1,2</sup> Huaixiang Wang,<sup>1,2</sup> Tahira Khan,<sup>1,2</sup> Furong Han,<sup>1,2</sup> Jine Zhang,<sup>1,2</sup> Hailin Huang,<sup>1,2</sup> Jing Zhang,<sup>1,2</sup> Hongrui Zhang,<sup>1,2</sup> Hui Zhang,<sup>1,2</sup> Xi Yan,<sup>1,2</sup> Shaojin Qi,<sup>1,2</sup> Fengxia Hu,<sup>1</sup> Baogen Shen,<sup>1</sup> Richeng Yu,<sup>1</sup> and Jirong Sun<sup>1,2,4,5,\*</sup>

<sup>1</sup>*Beijing National Laboratory for Condensed Matter Physics and Institute of Physics, Chinese Academy of Sciences, Beijing 100190, China*

<sup>2</sup>*School of Physical Sciences, University of Chinese Academy of Sciences, Beijing 100049, China*

<sup>3</sup>*Fujian Innovation Academy, Chinese Academy of Sciences, Fuzhou, Fujian 350108, China*

<sup>4</sup>*Songshan Lake Materials Laboratory, Dongguan, Guangdong 523808, People's Republic of China*

<sup>5</sup>*Spintronics Institute, University of Jinan, Jinan, Shandong 250022, People's Republic of China*

(Received 4 August 2019; revised manuscript received 26 September 2019; published 7 November 2019)

Tuning magnetic anisotropy (MA) by electric field is crucially important for the development of low-power-consumption magnetoelectric devices. In general, the MA is determined by magnetocrystalline anisotropy, magnetoelastic coupling, or exchange bias. We present an alternative approach that tunes the MA of the (110)-orientated  $\text{La}_{2/3}\text{Sr}_{1/3}\text{MnO}_3$  (LSMO) film by modulating the phase structure of its oxide cap layer. The LSMO layer exhibits a [1̄10] easy direction when it is capped by a  $\text{SrCoO}_{2.5}$  layer. Driving the cap layer to transit between the  $\text{SrCoO}_{2.5}$  and  $\text{SrCoO}_{3-\delta}$  phases via ionic-liquid gating, a bidirectional tuning between the [001] and [1̄10] directions is achieved for the MA of the LSMO layer. More importantly, the electric tuning of the MA is very reversible. Based on x-ray linear dichroism analysis, we show that the phase transition of  $\text{SrCoO}_x$  causes a variation of the electron population of the Mn 3d orbitals of LSMO, resulting in the MA switching of the MA of LSMO. The preferentially occupied orbital is  $d_{x^2-y^2}$  in  $\text{SrCoO}_{2.5}/\text{LSMO}$  and  $d_{3z^2-r^2}$  in  $\text{SrCoO}_{3-\delta}/\text{LSMO}$ . This work demonstrates a unique approach to reversibly tune the MA of LSMO, paving the way toward electrically tunable magnetoelectric devices based on correlated oxides.

DOI: 10.1103/PhysRevApplied.12.054016

## I. INTRODUCTION

Perovskite manganites with strongly correlated spin, orbital, charge, and lattice degrees of freedom have attracted great interest during past decades due to their abundant electronic and magnetic phenomena [1], such as the metal-insulator transitions accompanying magnetic phase transitions [2], colossal magnetoresistance effects [3,4], giant magnetocaloric effects [5], and effects associated with charge-orbital ordering [6]. Among others, magnetic anisotropy (MA) is a fundamental characteristic that directly affects the coercivity, magnetic domain structure, and spin switching dynamics [7–9].

In particular, it is of special importance to realize the electric control of MA, which will lead to low-power-consumption magnetoelectric devices [10–16]. As is well documented, the MA of a magnetic material can be classified into two categories. The first one is the intrinsic

magnetocrystalline anisotropy associated with crystal symmetry, and the second one is an extrinsic anisotropy arising from magnetoelastic coupling or interfacial spin pinning [17]. Much effort has been devoted to the electric tuning of these two kinds of MA, such as piezoelectrically distorting the ferromagnetic-piezoelectric hybrids [18], electrically amending the MA via magnetoelectric coupling in multiferroics [19,20], modulating carrier density to cause an electronic phase transition [21,22], and so on. These works are worthwhile because of their profound physical implications, for example, the strong magnetoelectric coupling in composite multiferroic systems based on charge modulation and the concept of electrically controlling the orbital degree of freedom in correlated electron systems.

$\text{La}_{2/3}\text{Sr}_{1/3}\text{MnO}_3$  (LSMO) exhibits a Curie temperature ( $T_C$ ) well above room temperature and is half metallic with nearly 100% spin polarization. It is, therefore, a model system for the exploration for emergent phenomena [23]. For bulk LSMO, the intrinsic magnetocrystalline anisotropy is approximately  $1.8 \times 10^4$  erg/cm<sup>3</sup> [24], much lower than

\*jrsun@iphy.ac.cn

†yschen@aphy.iphy.ac.cn

that of the conventional ferromagnetic metals such as Fe ( $4.8 \times 10^5$  erg/cm<sup>3</sup>) and Co ( $5 \times 10^6$  erg/cm<sup>3</sup>) [25]. For LSMO thin films, substrate-induced strains produce magnetoelastic effects, leading to a relatively large MA (approximately  $8.4 \times 10^4$  erg/cm<sup>3</sup>) [26]. The MA of LSMO film is closely related to the electron occupancy of Mn 3d orbitals [27,28], which strongly depends on the distortion of MnO<sub>6</sub> octahedra. In general, the in-plane tensile strain in (001) LSMO films favors the  $d_{x^2-y^2}$  occupancy and thus an easy plane MA, whereas the compressive strain favors  $d_{z^2}$  occupancy and a magnetic easy axis perpendicular to film plane anisotropy (PMA) [29]. Moreover, special octahedral rotations induced by interlayer coupling for heterostructures sometimes cause unexpected MA, for example, the controllable lateral MA in SrTiO<sub>3</sub>-buffered LSMO/NdGaO<sub>3</sub> films [30] and the spin reorientation in LSMO/SrIrO<sub>3</sub> superlattices [31]. In particular, the symmetry mismatch at the brownmillerite/perovskite (001) LaCoO<sub>x</sub>/LSMO interface can induce a PMA that is 2 orders of magnitude larger than that obtained by conventional magnetoelastic coupling [32].

A common feature of the above works is that the spin orientation is totally determined once the films or superlattices are formed. However, feasible approaches that can allow a reversible bidirectional switching of the MA are worthy of more investigation since they may lead to unforeseen alternative effects and potential applications. The reversible topotactic phase transition in SrCoO<sub>x</sub> (SCO<sub>x</sub>) under external stimuli gives us an inspiration to tune the spin orientation of SCO<sub>x</sub>-based bilayers. As is well established, brownmillerite- (BM) structured SrCoO<sub>2.5</sub> (SCO<sub>2.5</sub>), which consists of alternately stacked octahedral CoO<sub>6</sub> and tetrahedral CoO<sub>4</sub> planes, could be transformed to perovskite- (*P*) structured SrCo<sub>3-δ</sub> (SCO<sub>3-δ</sub>) by various methods, such as post annealing in an oxygen environment [33,34], wet chemical oxidizing [35], and ionic-liquid gating [36]. When SCO<sub>x</sub> forms a bilayer sample with a second oxide film, its phase transition will inevitably influence the latter oxide due to the presence of interlayer coupling. Based on this consideration, in this paper, we realize a reversible tuning to the MA of the LSMO film via tuning the phase structure of SCO<sub>x</sub>, which acts a cap layer for LSMO. The high-quality epitaxial (110)-orientated SCO<sub>2.5</sub>/LSMO bilayer films fabricated on (LaAlO<sub>3</sub>)<sub>0.3</sub>(SrAl<sub>0.5</sub>Ta<sub>0.5</sub>O<sub>3</sub>)<sub>0.7</sub> (LSAT) substrates are used as the model system. In this bilayer structure, the magnetic easy axis of LSMO is [1̄10]. We find that the positive (negative) electric ionic-liquid gating of the SCO<sub>2.5</sub> layer enhances (reduces) the magnitude of the MA of LSMO. More than that, reversible switching of the spin orientation between [001] and [1̄10] directions can be achieved by repeatedly reversing the polarity of the gating field, with the latter causing a reversible phase transition of SCO<sub>x</sub> between SCO<sub>2.5</sub> and SCO<sub>3-δ</sub>. X-ray linear dichroism analysis reveals a corresponding variation in Mn 3d

orbital occupancy for different SCO<sub>x</sub> phases, explaining the electric-field-induced switching of the MA. This work demonstrates a unique approach for the electric tuning of the MA of LSMO.

## II. EXPERIMENT

### A. Sample preparation and characterization

High-quality LSMO single-layer and SCO<sub>2.5</sub>/LSMO bilayer films are epitaxially grown on (110)-oriented LSAT ( $a = 3.868$  Å) substrates by the technique of pulsed laser deposition (PLD) utilizing a KrF excimer laser ( $\lambda = 248$  nm). The perovskite LSMO layer is first deposited at 730 °C in an oxygen pressure of 30 Pa with a laser fluence of 1.6 J/cm<sup>2</sup>. Then the SCO<sub>2.5</sub> layer is deposited at 700 °C in the oxygen pressure of 12 Pa with a laser fluence of 1.1 J/cm<sup>2</sup>. The film thickness is determined by deposition time. The deposition rate is calibrated by the technique of small-angle x-ray reflectivity (XRR, see Fig. S1 in the Supplemental Material [37]). Following this procedure, the superlattice samples of [SCO<sub>2.5</sub>(4u.c.)/LSMO(4u.c.)]<sub>5</sub> are also prepared for the x-ray linear dichroism measurement.

High-resolution x-ray diffraction (XRD) measurements have been performed using a D8 Discover diffractometer with Cu K $\alpha$  radiation. The lattice image of the heterointerface is investigated by a high-resolution scanning transmission electron microscope with double  $C_S$  correctors (STEM, JEOL-ARM200F). The chemical constitution of the bilayer is identified by energy dispersive x-ray spectroscopy (EDS). The magnetic properties are determined by carrying out measurements in a Quantum Design vibrating sample magnetometer superconducting quantum interference device (VSM SQUID) in the temperature range of 5–380 K. The magnetic field is applied along the [001] or [1̄10] axis of the (110) films. To perform ionic-liquid gating (ILG) experiments, a panel Pt/Ti/SiO<sub>2</sub>/Si substrate is used as the top electrode and the conductive LSMO layer is used as the bottom electrode [Fig. 3(a)]. The commercial, as-received ionic-liquid *N,N*-diethyl-*N*-(2-methoxyethyl)-*N*-methylammonium bis(trifluoromethylsulphonyl)imide is adopted in all ILG experiments. The ILG is performed at room temperature, and then the sample is cooled to the pre-set temperature for the measurements of magnetic loops. The thermomagnetic curve is collected in the cooling process after gating the sample at room temperature to the desired states.

The x-ray absorption spectroscopy (XAS) measurements are performed at the beamline BL08U1A in the Shanghai Synchrotron Radiation Facility at room temperature in a total electron yield mode. The spectra of Mn *L* edge are measured for the two polarizations of the linearly polarized x rays. As shown in the inset of Fig. 5, in normal incidence, vertically polarized x rays correspond

to the [001] direction ( $E \parallel [001]$ ,  $I_{[001]}$ ) and horizontally polarized x rays correspond to the [110] direction ( $E \parallel [1\bar{1}0]$ ,  $I_{[1\bar{1}0]}$ ). The spectral are normalized by dividing the experimental data by a factor, which makes the  $L_3$  pre-edge and  $L_2$  postedge have identical intensities for the two polarizations. After that, the pre-edge spectral region is set to zero and the peak at the  $L_3$  edge is set to unity. The x-ray linear dichroism (XLD) is the difference between the two measurements ( $I_{[001]} - I_{[1\bar{1}0]}$ ), which probes the Mn 3d orbital occupation in a LSMO single film or  $\text{SCO}_{2.5}$ /LSMO superlattice. Additionally, to confirm the occurrence of phase transition by ILG, the soft XAS spectra of Co  $L$  edge are collected for the  $\text{SCO}_{2.5}$ /LSMO bilayers in as-deposited, positively gated, and negatively gated states.

### III. RESULTS AND DISCUSSION

Two series of  $\text{SCO}_{2.5}$ /LSMO bilayer films are grown on (110) LSAT substrates by PLD. The first series of bilayers consists of a LSMO with a layer thickness between 4 and 10 nm and a fixed  $\text{SCO}_{2.5}$  layer of 10 nm. The second series of samples has a fixed LSMO thickness of 6 nm, but different  $\text{SCO}_{2.5}$  thicknesses varying from 1 to 10 nm. For comparison, LSMO single-layer films with thicknesses

ranging from 4 to 10 nm are also fabricated on (110) LSAT substrates. Here, the (110) films instead of the (001) films are adopted because of the presence of uniaxial strains in the former films, which makes an in-plane magnetic switching between [001] and [110] electrically tunable. For the (001) films, the two in-plane directions [001] and [010] are equivalent. Tuning SCO will not affect in the in-plane magnetic orientation.

All samples exhibit good crystallinity and layer-by-layer epitaxial growth as confirmed by the TEM pattern and XRD spectra. The cross-section high-angle annular dark-field (HAADF) image and corresponding EDS elemental mapping of  $\text{SCO}_{2.5}(10 \text{ nm})/\text{LSMO}(5 \text{ nm})$  films are illustrated in Figs. 1(a) and 1(b). The sharp interface between the top  $\text{SCO}_{2.5}$  and bottom LSMO is clearly demonstrated. Moreover, alternate and parallel dark stripes with an inclination angle of  $45^\circ$  to the film plane are observed in the  $\text{SCO}_{2.5}$  layer. This is the typical feature of a BM structure: the dark stripes represent the tetrahedral  $\text{CoO}_4$  planes with relatively larger Sr-Sr atomic spacing compared to that of the octahedral  $\text{CoO}_6$  planes. Thus, the inclined dark stripes unambiguously confirm that the  $\text{CoO}_4$  and  $\text{CoO}_6$  planes are alternately stacked along one of the [100] and [010] axes for the (110)-oriented  $\text{SCO}_{2.5}$  films, which is

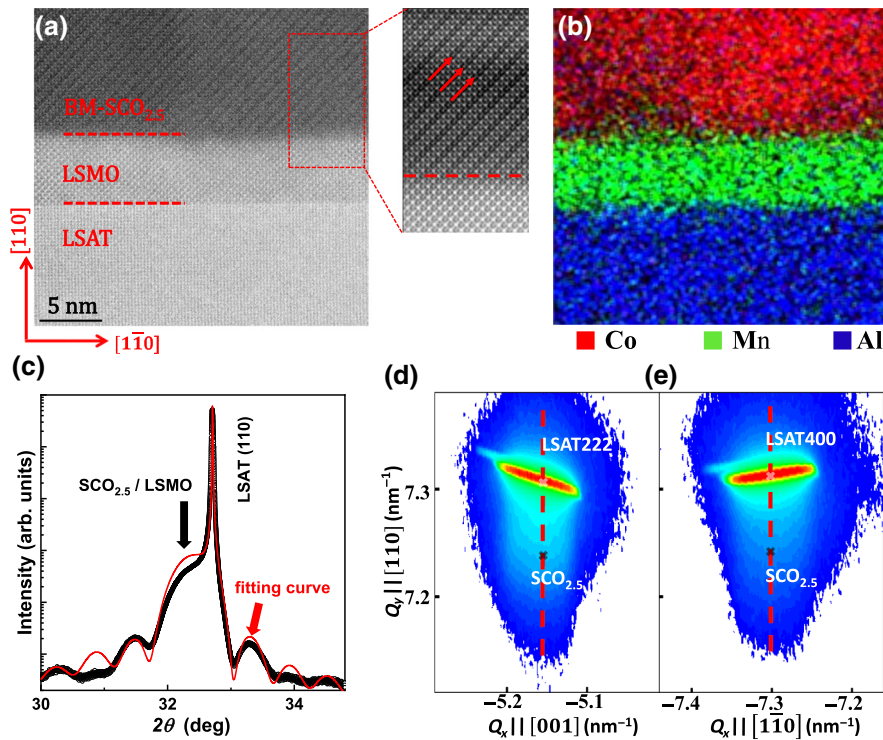


FIG. 1. (a) The HAADF image of the cross section of a (110)  $\text{SCO}_{2.5}(10 \text{ nm})/\text{LSMO}(5 \text{ nm})/\text{LSAT}$  bilayer recorded along the [001] zone. The lattice image of the  $\text{SCO}_{2.5}$  layer shows alternate and parallel dark stripes with an inclination angle of  $45^\circ$  to the film plane (marked as red arrows), indicating the brownmillerite superstructure is along the [100] or [010] axis. (b) Chemical constitution of each layer measured by EDS elemental mapping. (c) The out-of-plane  $\theta$ - $2\theta$  pattern of a (110)  $\text{SCO}_{2.5}(10 \text{ nm})/\text{LSMO}(10 \text{ nm})$  film. It can be well fitted by the diffraction-interference model of x rays within a bilayer structure (red curve). The in-plane lattice parameters along the [001] and [110] directions are revealed by the RSMs of the (d) (222) and (e) (400) reflections.

consistent with the XRD measurements given in our previous work [38]. Different from  $\text{SCO}_{2.5}$ , the LSMO layer shows the typical perovskite structure in a HAADF image. It also indicates that half of the  $\text{MnO}_6$  octahedra at the interface are connected to the  $\text{CoO}_4$  tetrahedra.

Figure 1(c) presents the out-of-plane  $\theta$ - $2\theta$  scan of a  $\text{SCO}_{2.5}(10 \text{ nm})/\text{LSMO}(10 \text{ nm})$  film, showing clear thickness fringes around the (110) main peak. These multiple peaks suggest a high degree of interface abruptness in the film that can be well fitted by the diffraction-interference process of x rays with a bilayer structure. To determine the in-plane lattice parameters, the reciprocal space mappings (RSM) of the (222) and (040) reflections of the  $\text{SCO}_{2.5}/\text{LSMO}$  film are collected as shown in Figs. 1(d) and 1(e). We can see that the diffraction peaks of the  $\text{SCO}_{2.5}/\text{LSMO}$  film (marked by dark crosses) are strictly located below that of the LSAT substrate in either the [001] or [110] direction, indicating the bilayer films are coherently strained to the underlying substrate. According to previous reports, the lattice parameter of bulk LSMO is

3.876 Å, which is slightly larger than that of the LSAT substrate (3.868 Å) [39]. As shown by the RSM results, there is no lattice relation. This means that the LSMO layer within the bilayer structure suffers from a weak compressive stress along the in-plane [001] axis, the same as the bare LSMO/LSAT films.

Before electric tuning, we will show the initial characteristics of the BM/P heterointerface. The most remarkable observation is that the  $\text{SCO}_{2.5}/\text{LSMO}$  bilayer films display an abnormal in-plane MA, opposite to the LSMO single films with equivalent stress. To demonstrate this feature more clearly, in Fig. 2(a), we show the temperature-dependent magnetization ( $M$ - $T$ ) of the  $\text{SCO}_{2.5}(10 \text{ nm})/\text{LSMO}(t \text{ nm})$  bilayers with the LSMO thickness varying from 4 to 10 nm, measured in a low magnetic field (0.01 T) applied along the [001] or [110] axis. For comparison, the  $M$ - $T$  curves of the LSMO single film with equivalent thickness are also given in Fig. S2 (see in the Supplemental Material [37]). For the  $\text{SCO}_{2.5}/\text{LSMO}$  bilayers, the magnetic moments are basically isotropic

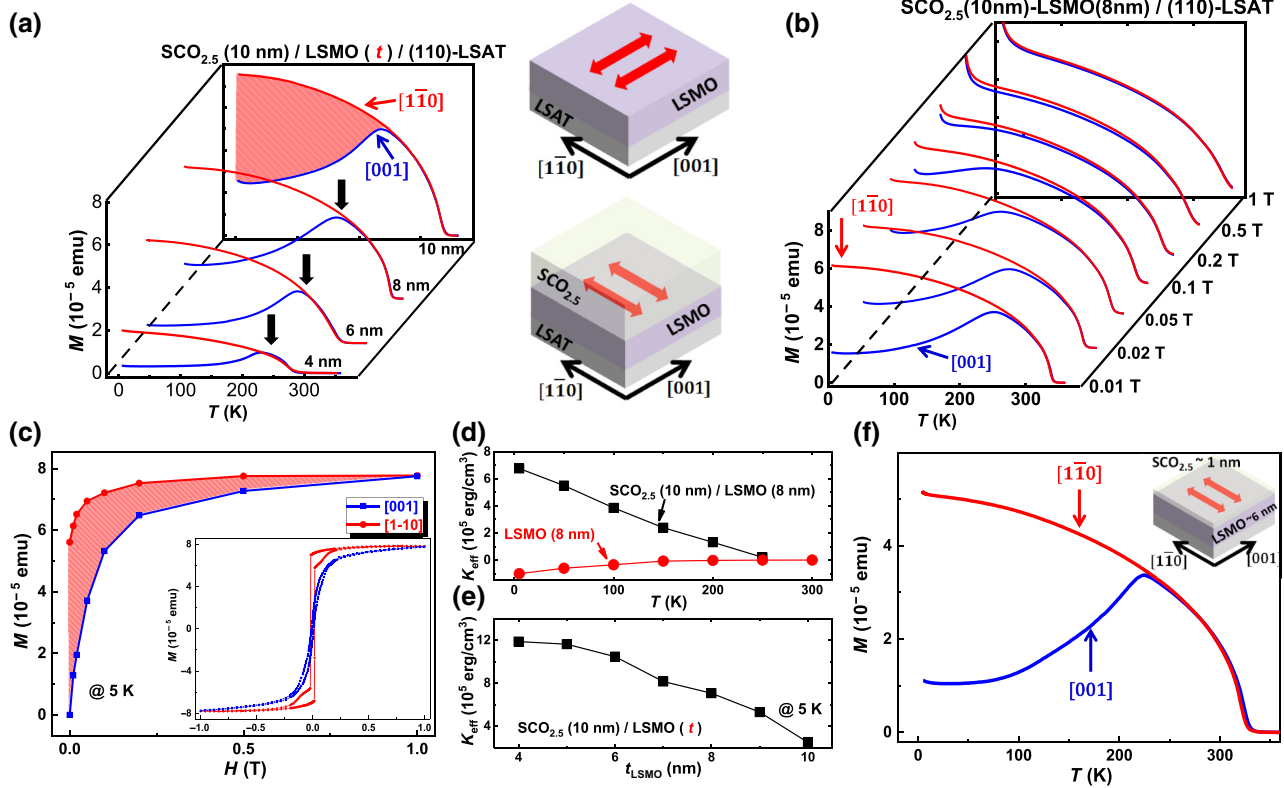


FIG. 2. (a)  $M$ - $T$  curves for the  $\text{SCO}_{2.5}(10 \text{ nm})/\text{LSMO}(t \text{ nm})$  bilayers with LSMO thicknesses ranging from 4 to 10 nm. Two  $M$ - $T$  curves are acquired in field-cooling mode for each sample, with a magnetic field (approximately 0.01 T) applied along the [001] or [110] axis. Black arrows indicate the critical temperature of spin reorientation. Insets are the schematic views of the magnetic easy axis (indicated by red double arrows) for the bare LSMO film and the  $\text{SCO}_{2.5}/\text{LSMO}$  bilayers. (b)  $M$ - $T$  curves for a  $\text{SCO}_{2.5}(10 \text{ nm})/\text{LSMO}(8 \text{ nm})$  bilayer film measured under different magnetic fields (0.01–1 T). (c) Magnetic moment as a function of magnetic field extracted from the  $M$ - $T$  curves in (b) at  $T = 5 \text{ K}$ . The shaded area corresponds to the in-plane MA energy that is consistent with the direct measurements of magnetic loops shown in the inset. (d) Temperature dependence of anisotropy constant ( $K_{\text{eff}}$ ) of the  $\text{SCO}_{2.5}(10 \text{ nm})/\text{LSMO}(8 \text{ nm})$  bilayer and LSMO(8 nm) single films. (e) The variation of  $K_{\text{eff}}$  of the  $\text{SCO}_{2.5}(10 \text{ nm})/\text{LSMO}(t \text{ nm})$  bilayers on the LSMO thickness. (f)  $M$ - $T$  curves for a  $\text{SCO}_{2.5}(1 \text{ nm})/\text{LSMO}(6 \text{ nm})$  bilayer film, with a magnetic field applied along the [001] or [110] axis.

in the film plane at the high-temperature region. Interestingly, an abnormal spin reorientation occurs in the [001]  $M$ - $T$  curves when the temperature is reduced to a critical value, ranging from 230 to 250 K depending on the LSMO thickness. This spin reorientation causes a rapid decrease of magnetic moment in the [001] orientation that becomes much lower than that obtained in the [1̄10] direction. Combining the  $M$ - $T$  curve measured in the out-of-plane [110] direction (see Fig. S3 in the Supplemental Material [37]), we can conclude that the magnetic easy axis of  $\text{SCO}_{2.5}/\text{LSMO}$  bilayers prefers to lie along the in-plane [110] direction. As  $\text{SCO}_{2.5}$  is a  $G$ -type antiferromagnetic insulator that has no contribution to the low-field magnetization measurements [40], the considerable MA of  $\text{SCO}_{2.5}/\text{LSMO}$  bilayers should all originate from the LSMO layer. This is particularly interesting because the bare LSMO layers on the (110) LSAT substrate demonstrate a [001] easy axis (see Fig. S2 in the Supplemental Material [37]), although it is constrained to the same state as the bilayers. That is to say, the magnetic moment of the bottom LSMO layer has been rotated by 90° in the film plane, from the [001] to the [1̄10] direction, by simply capping a BM- $\text{SCO}_{2.5}$  layer.

Figure 2(b) shows the typical features of  $M$ - $T$  curves measured under different magnetic fields for a  $\text{SCO}_{2.5}(10 \text{ nm})/\text{LSMO}(8 \text{ nm})$  film. We can see that the difference between the [001] and [1̄10]  $M$ - $T$  curves is more obvious under lower fields. This is reasonable since the large applied field would align all magnetic moments in the same direction, overcoming the MA. We extract the magnetization  $M$  at 5 K from these  $M$ - $T$  curves and plot it as a function of magnetic field  $H$  in Fig. 2(c). The red-shaded area enclosed by the two  $M$ - $H$  relations thus provides a quantitative estimation of the MA energy of the bilayer. The calculated anisotropy constant ( $K_{\text{eff}}$ , where the positive sign implies the easy axis along the [1̄10] direction) is as large as  $7.4 \times 10^5 \text{ emu/cm}^3$  at 5 K, far exceeding the conventional anisotropy energy caused by magnetoelastic coupling ( $8.4 \times 10^4 \text{ erg/cm}^3$ ) or magnetocrystalline anisotropy ( $1.8 \times 10^4 \text{ erg/cm}^3$ ) of LSMO [24, 26]. This anisotropy constant is consistent with the value estimated from the direct measurements of magnetic loops ( $6.7 \times 10^5 \text{ emu/cm}^3$ ) as shown in the inset of Fig. 2(c). We perform similar calculations at other temperatures and present the dependence of  $K_{\text{eff}}$  on temperature in Fig. 2(d). As expected,  $K_{\text{eff}}$  continuously decreases with the increase in temperature and finally vanishes around the critical temperature of spin reorientation. The anisotropy constant of the LSMO/LSAT single film with the same thickness of 8 nm is also calculated, which gives a negative and much smaller  $K_{\text{eff}}$  of about  $-1.0 \times 10^5 \text{ erg/cm}^3$  at 5 K. Figure 2(e) shows the anisotropy constant as a function of the LSMO thickness. The  $K_{\text{eff}}$  is maximal (approximately  $1.2 \times 10^6 \text{ erg/cm}^3$ ) when the LSMO layer thickness is 4 nm. It displays a monotonical decrease with the

increase in LSMO thickness. This is a typical feature for the interface-induced MA, strongly suggesting the effect of  $\text{SCO}_{2.5}/\text{LSMO}$  interface coupling on the spin reorientation. We also investigate the influence of the  $\text{SCO}_{2.5}$  thickness on MA for the bilayer films, fixing the LSMO thickness to 6 nm. Interestingly, even a  $\text{SCO}_{2.5}$  layer of approximately 1 nm in thickness has the effect of aligning the magnetic easy axis of LSMO along [1̄10] [Fig. 2(f)]. Clearly, it is the nearest-neighbor  $\text{SCO}_{2.5}$  layer that results in the abnormal MA.

Subsequently, we will turn our attention to the electrical manipulation of the MA of  $\text{SCO}_{2.5}/\text{LSMO}$ . As is well documented, the one-dimensional oxygen vacancy channels within BM- $\text{SCO}_{2.5}$  provide favorable conditions for ionic diffusion and valence change of cobalt ions. The electric-field-controlled topotactic phase transformation between three distinct phases,  $\text{SrCoO}_{2.5}$ ,  $\text{SrCoO}_{3-\delta}$ , and  $\text{HSrCoO}_{2.5}$ , has already been achieved by Lu *et al.* using the ILG method at room temperature [36]. Inspired by the critical role of the interface coupling for the MA of  $\text{SCO}_{2.5}/\text{LSMO}$  bilayers, we are interested in what the consequences will be if the phase of the cap layer is changed. We set up the electric tuning experiment of the bilayer films as shown in Fig. 3(a). According to former works of ILG, the positive or negative bias would, respectively, introduce hydrogen or oxygen ions into the  $\text{SCO}_x$  layer, causing complex changes in atomic structure and the valence state of Co ions. Moreover, since  $\text{SCO}_x$  has a much higher ionic mobility than LSMO, by using an appropriate bias voltage and gating time, we can ensure that the gating effect mainly influences the top  $\text{SCO}_x$  layer and slightly affects the underneath LSMO, which is proven by the unchanged  $T_C$  provided in later discussions.

Figure 3(b) is the *in situ* XRD spectra taken during the ILG process for the  $\text{SCO}_{2.5}(10 \text{ nm})/\text{LSMO}(8 \text{ nm})$  bilayer. The  $\theta$ - $2\theta$  scanning is performed for the (100) planes, obtained by rotating the sample anticlockwise around the [001] axis by approximately 45° as shown in the inset of Fig. 3(b) [38]. The (200) diffraction peak of the initial film with the  $\text{SCO}_{2.5}$  BM phase (at around 46.2°) is localized on the left side of the LSAT substrate. After a gating of 5 min by a +3 V bias, this peak disappears and a new peak appears at about 44.4°, exactly corresponding to the  $\text{HSCO}_{2.5}$  phase as reported by Lu *et al.* [36]. Furthermore, if a negative bias of -2.7 V is applied to the  $\text{HSCO}_{2.5}$  phase for 7 min, the  $\text{SCO}_{2.5}$  peak is partially restored and a small peak at about 47.4° appears, which indicates the occurrence of the perovskite  $\text{SCO}_{3-\delta}$  phase. The effectiveness of ILG for the bilayer structure is also confirmed by the soft XAS spectrum at the cobalt  $L$  edge as shown in Fig. 3(c). The peak position of  $\text{Co } L_3$  shifts from 777.2 to 775.7 eV after the positive ILG, suggesting a decrease in the valence of cobalt ions by the insertion of  $\text{H}^+$  ions. In contrast, the negative gating would insert  $\text{O}^{2-}$  ions into the

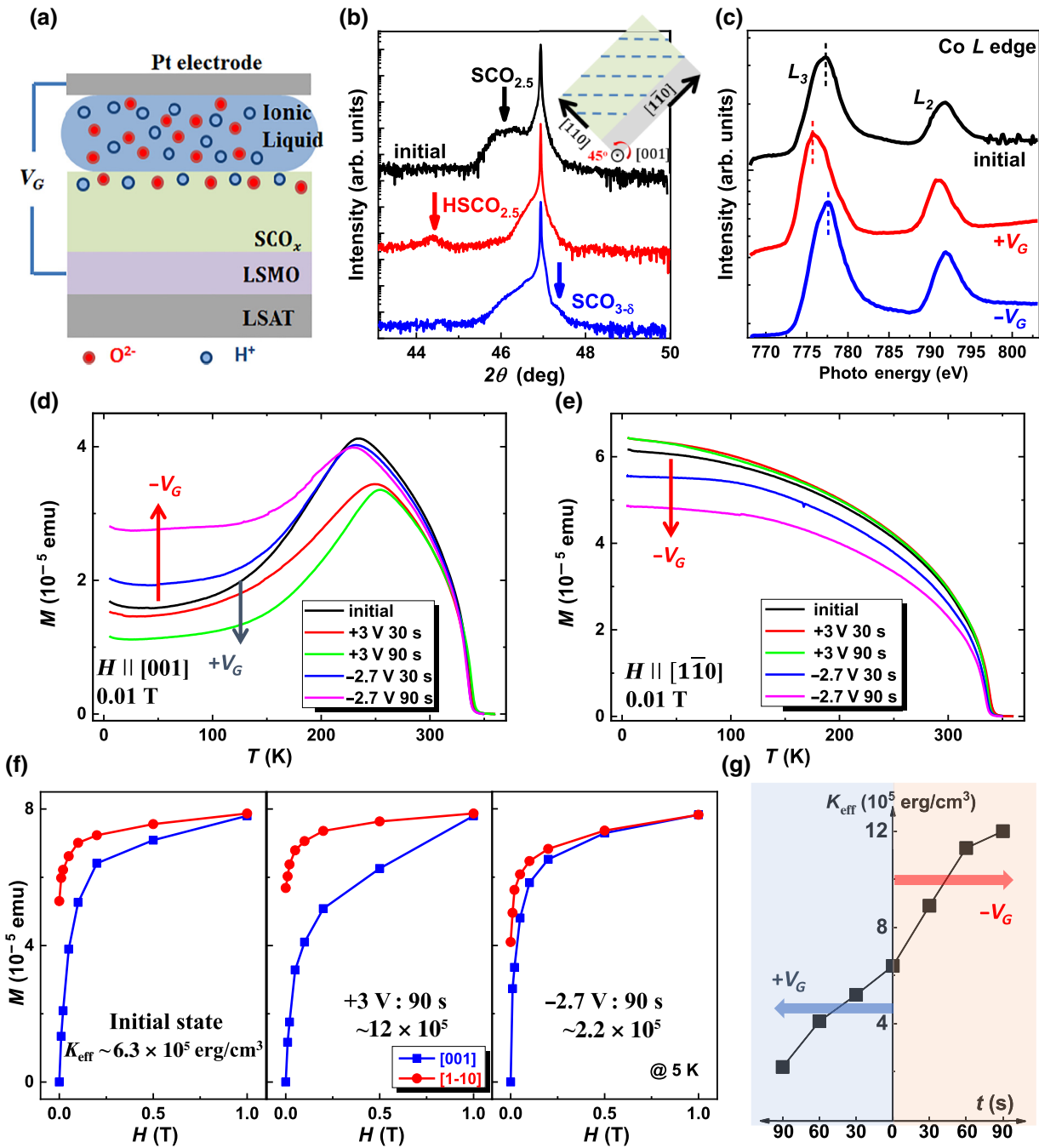


FIG. 3. (a) Experimental setup of ionic-liquid gating performed on the  $\text{SCO}_{2.5}/\text{LSMO}$  bilayers. (b) *In situ* XRD spectra of the (110)  $\text{SCO}_{2.5}/\text{LSMO}$  bilayer film, reflected from the (100) lattice planes (by rotating the sample anticlockwise around the [001] axis at approximately  $45^\circ$  as shown in the inset). (c) Soft XAS spectra of Co  $L$  edges for a bilayer film in the initial, positively gated, and negatively gated states. Compared with the initial state, the peak position of the Co  $L$  edge shifts toward lower energy (or higher energy) in positive (or negative)  $V_G$  biasing. (d)  $M$ - $T$  curves for a  $\text{SCO}_{2.5}(10 \text{ nm})/\text{LSMO}(8 \text{ nm})$  bilayer film measured in different electric tuning states, with a magnetic field applied in-plane along the [001] or (e) [110] direction. (f) The calculated anisotropy strength in different electric tuning states for the same film at  $T = 5 \text{ K}$ . (g) The dependence of  $K_{\text{eff}}$  on biasing time in positive (left-half axle) or negative (right-half axle) gating.

$\text{SCO}$  layer, causing the shift of the  $L_3$  peak toward a higher energy of  $777.6 \text{ eV}$ .

The XRD and XAS results prove the reversible electric tuning of the  $\text{SCO}_x$  cap layer between different

phases. A natural issue is its effect on neighboring  $\text{LSMO}$  because of the  $\text{SCO}_{2.5}/\text{LSMO}$  interface coupling. To highlight the variation of the  $\text{LSMO}$  layer, we first focus on the short-term ILG experiments, avoiding

additional magnetic signals from ferromagnetic  $\text{SCO}_{3-\delta}$  or weak ferromagnetic  $\text{HSCO}_{2.5}$  phases. Two identical  $\text{SCO}_{2.5}(10 \text{ nm})/\text{LSMO}(8 \text{ nm})$  films are tuned under +3 and -2.7 V electrical biases, respectively. The variation trends of the [001] and [1̄1̄0]  $M$ - $T$  curves (under an applied field of 0.01 T), from the initial state to different gated states (30, 60, and 90 s), are summarized in Figs. 3(d) and 3(e). Obviously, for the [001] direction, the positive gating enhances spin reorientation, resulting in a gradual increase in critical temperature and reduced magnetization. Correspondingly, magnetization along the [1̄1̄0] direction is slightly enhanced. In contrast, the negative gating produces opposite effects as revealed by the increase and/or decrease in magnetizations along the [001] and/or [1̄1̄0] directions. As the  $T_C$  in all gated states is nearly the same as that of the initial film, we believe that the LSMO layer is almost untouched by the short-term ILG, and the variation of  $M$ - $T$  curves implies a change of the MA of the LSMO layer. Figure 3(f) provides a comparison of the  $M$ - $H$  relations at 5 K for the same bilayer film in the initial, positive, and negative gated states. The anisotropy constant  $K_{\text{eff}}$  varies from  $6.4 \times 10^5$  to  $1.2 \times 10^6 \text{ erg/cm}^3$  after a 3-min gating by a positive bias. On the contrary, it decreases to  $2.2 \times 10^5 \text{ erg/cm}^3$  after a 3-min negative gating. The calculated  $K_{\text{eff}}$  for different gated states is summarized in Fig. 3(g). It clearly shows the variation of MA under ILG, suggesting a tuning of structure coupling at the  $\text{SCO}_x/\text{LSMO}$  interface. As mentioned above, the positive ILG would insert  $\text{H}^+$  ions into the SCO layer and lower the valence state of the cobalt ions. It may enhance the lattice distortion of  $\text{CoO}_4$  tetrahedrons and further tilt the adjacent  $\text{MnO}_6$  octahedrons near the interface [36]. Thus, a larger MA of the LSMO layer is demonstrated. On the other hand, the insertion of  $\text{O}^{2-}$  ions into BM SCO would apparently reduce the proportion of  $\text{CoO}_4$  tetrahedrons at the interface, which affects the interface coupling, and thus the MA.

The above results further suggest that the direct connections of  $\text{CoO}_4\text{-MnO}_6$  at the interface are crucially important for the abnormal MA of the  $\text{SCO}_x/\text{LSMO}$  bilayers. The insertion of  $\text{O}^{2-}$  ions for 90 s has reduced the initial  $K_{\text{eff}}$  by two thirds. One natural expectation is the switching of the magnetic easy axis from [1̄1̄0] to [001] if the gating time is long enough. Figure 4(a) shows the [001] and [1̄1̄0]  $M$ - $T$  curves of a  $\text{SCO}_{2.5}(6 \text{ nm})/\text{LSMO}(6 \text{ nm})$  film in the initial state and a negative gated state (-2.7 V bias for 5 min) (for more details, see Fig. S4 in the Supplemental Material [37]). After the long-term negative ILG, two magnetic transition temperatures can be identified in the  $M$ - $T$  curves: the higher one of 307 K is the  $T_C$  of the LSMO layer, whereas the lower one near 100 K represents the paramagnetic-ferromagnetic transition of the  $\text{SCO}_x$  layer. According to ref. [36], it indicates that the major phase of the  $\text{SCO}_x$  layer now belongs to the perovskite type, that is,  $\text{SCO}_{3-\delta}$ .

The highlight of these two sets of  $M$ - $T$  curves is that, unlike the magnetic easy axis along the [1̄1̄0] direction for the  $\text{SCO}_{2.5}/\text{LSMO}$  bilayer, it turns to the [001] direction for the  $\text{SCO}_{3-\delta}/\text{LSMO}$  heterostructure in a temperature ranging from 250 to 50 K. There is a crossover of the [001] and [1̄1̄0]  $M$ - $T$  curves of the  $\text{SCO}_{3-\delta}/\text{LSMO}$  bilayer at about 50 K. This may be caused by the ferromagnetic contribution of the  $\text{SCO}_{3-\delta}$  layer that prefers to lie along the [1̄1̄0] direction at low temperature. According to the above analysis, a schematic diagram of the electrically controllable MA in  $\text{SCO}_x/\text{LSMO}$  bilayers is given in Fig. 4(b). Accompanied by the phase transformation of the  $\text{SCO}_x$  cap layer, the orientation of MA for the bottom LSMO layer is changed accordingly. More importantly, the electric tuning of the easy magnetic axis of the LSMO layer is reversible since the topotactic phase transformation is reversible. As shown in Fig. 4(c), a series of -2.7 and +2 V biases, with durations of 5 and 4 min, respectively, are alternately applied to the bilayer films. The  $M$ - $H$  curves are recorded for the initial state and each gating state, where the temperature is set to 140 K to exclude the magnetic signals from  $\text{SCO}_{3-\delta}$ . Although the MA energy is relatively smaller than that obtained at 5 K, the reversible switching of the magnetic easy axis between the [001] and [1̄1̄0] directions is confirmed. Figure 4(d) presents the calculated  $K_{\text{eff}}$  when the sample repeatedly switches between  $\text{SCO}_{2.5}/\text{LSMO}$  and  $\text{SCO}_{3-\delta}/\text{LSMO}$ .

As is well established, the MA of the LSMO is directly determined by the electron occupancy of  $\text{Mn}(d_{x^2-y^2}/d_{3z^2-r^2})$  orbitals. According to the Bruno model, the spin of Mn ions prefers to take the direction of the orbital momentum [27,28]. Thus, the reversible tuning of the orientation of the magnetic easy axis of the LSMO layer possibly implies that the orbital occupancy is modulated by the electric field. We then collect the XLD spectra, which is a sensitive probe of orbital occupancy, for the samples with different MAs. Details for the XLD measurement are given in Sec. II. Note the fact that, for (110) films, the in-plane [001] and [1̄1̄0] directions are parallel to the  $d_{3z^2-r^2}$  and  $d_{x^2-y^2}$  orbitals, respectively. Thus, the spectral intensity of  $I_{[001]}$  and  $I_{[1̄1̄0]}$  should be proportional to the hole occupancies of the  $d_{3z^2-r^2}$  and  $d_{x^2-y^2}$  orbitals.

The normalized XAS spectra with two polarizations and the corresponding XLD spectra ( $I_{[001]} - I_{[1̄1̄0]}$ ) are illustrated in Figs. 5(a)-5(c) for a single LSMO film and prime and negatively gated  $[\text{SCO}_{2.5}(4\text{u.c.})/\text{LSMO}(4\text{u.c.})]_5$  superlattices, respectively. (Here, the superlattice is used instead of the bilayer film to highlight the interface effect.) As reported, the difference in  $L_2$  peaks (648–660 eV) measured with two polarized lights can provide the information on  $e_g$  orbital occupancy. The integrated area of the LSMO single film gives a positive value, indicating that the  $d_{3z^2-r^2}$  orbital is preferentially occupied. In contrast, for the prime  $[\text{SCO}_{2.5}/\text{LSMO}]_5$  superlattice, the XLD spectrum exhibits a negative peak around  $L_2$ , indicating that  $d_{x^2-y^2}$

is the favorable orbital. However, when  $[SCO_{2.5}/LSMO]_5$  is transformed into  $[SCO_{3-\delta}/LSMO]_5$  by ILG, the  $d_{3z^2-r^2}$  orbital becomes the preferred orbital again as indicated by the positive XLD peak around  $L_2$ . It is, therefore, clear that the ILG tunes the magnetic anisotropy by modifying the orbital population for  $SCO_x/LSMO$  bilayer films. This result is particularly interesting in the sense that it reveals the possibility to tune interface reconstruction and thus orbital occupancy by an external electric field in oxide heterostructures.

To understand the reversible tuning of orbital occupancy and the consequent MA, a simple phenomenological model is proposed in Figs. 5(d) and 5(e). As mentioned

above, although the LSMO/LSAT single film suffers from a small compressive stress along the in-plane [001] direction, the magnetic easy axis of the LSMO is still aligned along the [001] axis, which is similar to results of previous works [41–43]. It is possible that the MA is determined by oxygen octahedral rotations and distortions due to uniaxial strains in the films. For the (110)- $SCO_{2.5}/LSMO$  bilayers, it is totally different. The regular dark stripes identified in the STEM image indicate that half of the  $MnO_6$  octahedra are connected with the  $CoO_4$  tetrahedra at the (110) BM/P-type interface. As already demonstrated in previous work [34], the oxygen-deficient  $CoO_4$  sublayers would cause local structural changes in the adjacent  $CoO_6$

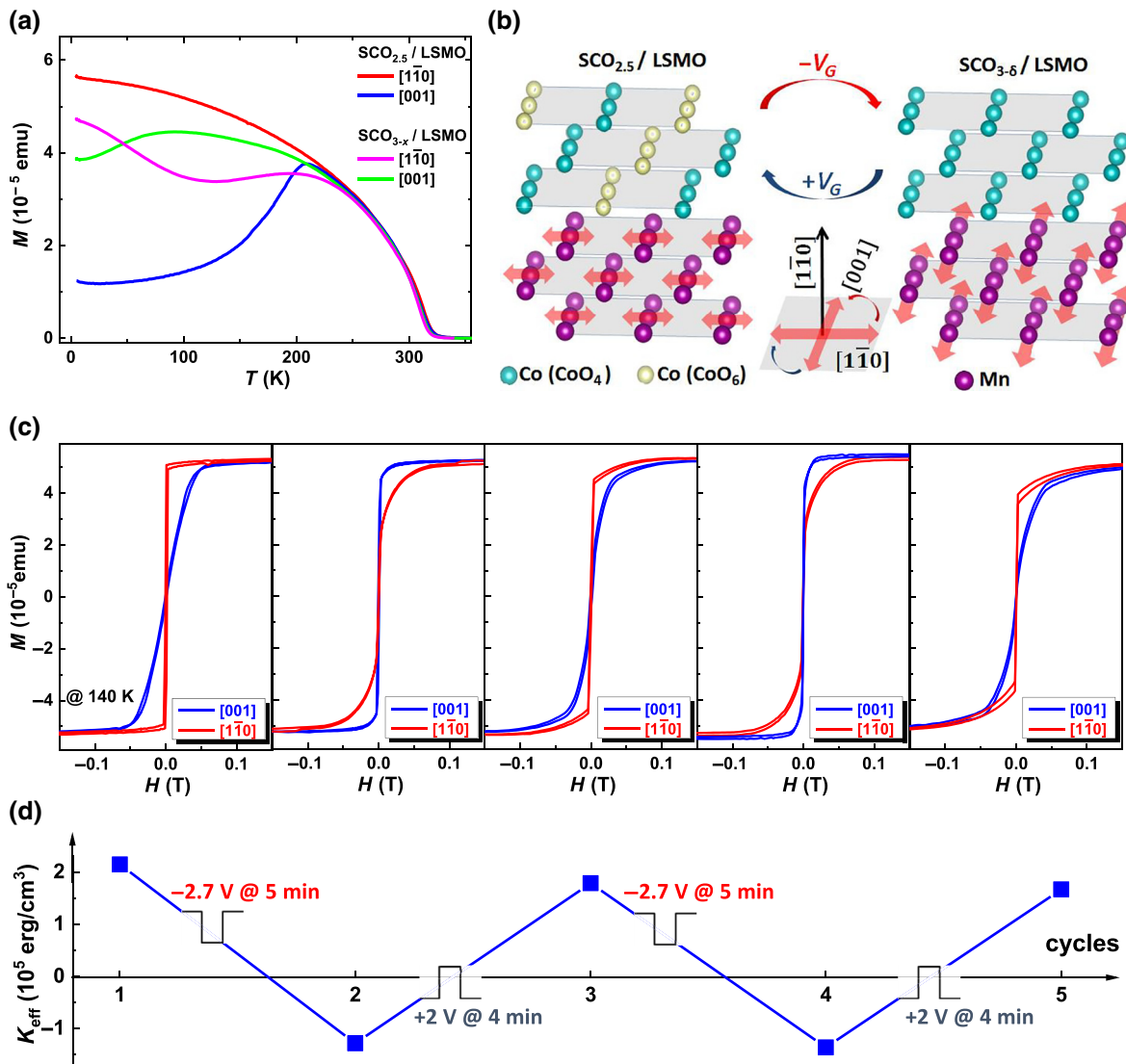


FIG. 4. (a)  $M$ - $T$  curves for a  $SCO_{2.5}(6 \text{ nm})/LSMO(6 \text{ nm})$  bilayer film measured in the initial state and after negative ILG for 5 min. (b) Schematic model of the spin structure of the LSMO layer at  $SCO_{2.5}/LSMO$  and  $SCO_{3-\delta}/LSMO$  interfaces. By reversibly switching the phases of the  $SCO_x$  top layer, the magnetic easy axis of the LSMO layer is tuned by the electric bias accordingly. (c)  $M$ - $H$  curves in the  $[001]$  and  $[1\bar{1}0]$  directions for the same  $SCO_{2.5}(6 \text{ nm})/LSMO(6 \text{ nm})$  bilayer film during the repeated electric tuning cycles, measured at  $T = 140$  K. (d) The corresponding  $K_{\text{eff}}$  calculated in each state, demonstrating the opposite sign after the alternately applied positive and negative gateings.

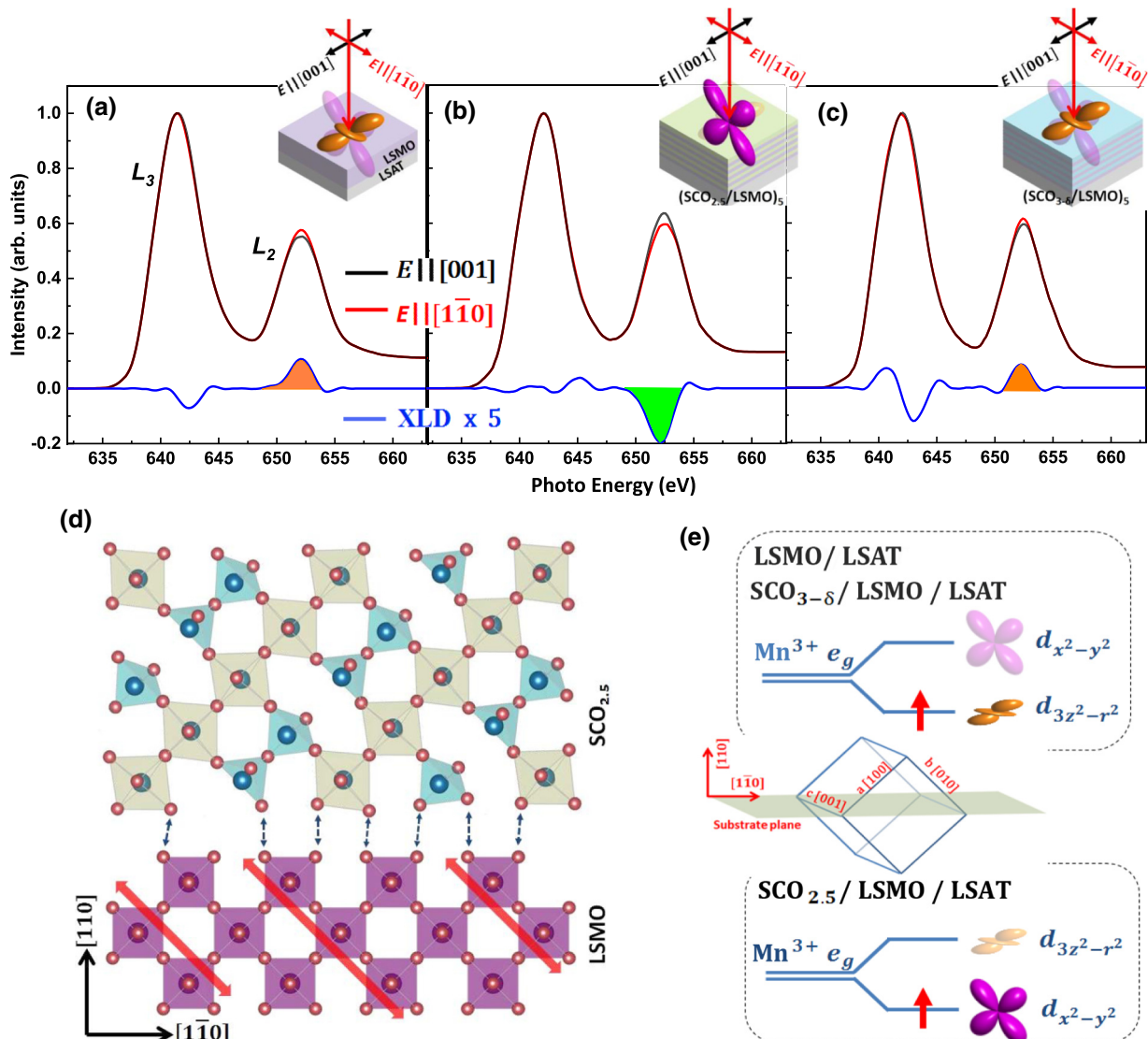


FIG. 5. Normalized XAS spectra for (a) the LSMO single film, (b) as-deposited [SCO<sub>2.5</sub>(4u.c.)/LSMO(4u.c.)]<sub>5</sub> superlattice and (c) negatively gated [SCO<sub>2.5</sub>(4u.c.)/LSMO(4u.c.)]<sub>5</sub> superlattice, measured with the polarized x-ray beam with different incident angles (see Sec. II). The deduced XLD spectrum ( $I_{[001]} - I_{[1\bar{1}0]}$ ) is given by the black line below. Its integration over the energy range from 648 to 660 eV (around the  $L_2$  edge) of the LSMO single film gives a positive value, indicating the  $d_{3z^2-r^2}$  occupancy. For the initial [SCO<sub>2.5</sub>(4u.c.)/LSMO(4u.c.)]<sub>5</sub> superlattice, the negative XLD signal confirms the  $d_{x^2-y^2}$  occupancy. After the electric tuning under negative bias, the XLD signal of the [SCO<sub>2.5</sub>(4u.c.)/LSMO(4u.c.)]<sub>5</sub> superlattice turns to a positive value as does the LSMO single film, which means the orbital occupancy is changed from  $d_{x^2-y^2}$  to  $d_{3z^2-r^2}$ . (d) Schematic model of atomic ordering of the (110) SCO<sub>2.5</sub>/LSMO film. The direct connections of CoO<sub>4</sub>-MnO<sub>6</sub> at the interface would elongate and tilt the MnO<sub>6</sub> octahedra along the superstructure direction as marked by red arrows. (e) Representation of the effect of the MnO<sub>6</sub> octahedral distortions on the  $e_g$  orbital occupation of Mn<sup>3+</sup>. The LSMO single or SCO<sub>3-δ</sub>/LSMO film favors  $d_{3z^2-r^2}$  occupancy, whereas it turns to  $d_{x^2-y^2}$  occupancy in the SCO<sub>2.5</sub>/LSMO bilayer.

sublayers. The O-O distance of CoO<sub>6</sub> octahedra is significantly elongated along the CoO<sub>4</sub>/CoO<sub>6</sub> stacking direction, from 3.83 Å for *P*-SCO<sub>3-δ</sub> to 4.40 Å for BM-SCO<sub>2.5</sub>. When the MnO<sub>6</sub> octahedra are directly connected to the CoO<sub>4</sub> tetrahedra at the SCO<sub>2.5</sub>/LSMO interface, a similar effect may elongate the MnO<sub>6</sub> octahedra along the superstructure direction of the SCO<sub>2.5</sub> cap layer, that is, the [100]

or [010] axis in different domains. This elongation is much stronger than that induced by the substrate strain, which would cause the preferred occupation of the  $d_{x^2-y^2}$  orbital and the rotation of the magnetic easy axis to the [1̄10] direction as shown in Fig. 5(e). Moreover, the insertion of H<sup>+</sup> ions into SCO<sub>2.5</sub> would increase the strontium-strontium atomic distance in the tetrahedral sublayers [36].

This will further enhance the elongation and tilting of  $\text{MnO}_6$  octahedrons near the interface, resulting in a larger MA. In contrast, the introduction of  $\text{O}^{2-}$  ions into  $\text{SCO}_{2.5}$  has the opposite effect, resulting in the  $\text{CoO}_6\text{-MnO}_6$  interface that favors the [001] easy axis as for LSMO single films. All these results suggest that the unique structure coupling at the brownmillerite/perovskite interface plays the key role in the tunable magnetic anisotropy. It was already known that the topotactic reduction of perovskite oxides could be also realized in ferrates and nickelates, resulting in a series of brownmillerite or even “infinite layer” oxides [44,45]. Thus, the principle proven here may be extended to the combinations of these perovskitelike oxides with LSMO, introducing alternative functionalities or emergent phenomena into the correlated oxide heterojunctions.

Finally, we mention the importance of the present demonstration and some possible applications in magnetoelectronics or spintronics. Different from the electrical modulation of magnetism in ferromagnetic metals [11–14], the electrical tuning of MA in  $\text{SCO}_x/\text{LSMO}$  bilayers is nonvolatile since the topotactic phase transition of the  $\text{SCO}_x$  cap layer is quite stable at room temperature. Thus, it could be regarded as a field-effect memory magnet, where the magnet can be reversibly tuned between two distinct magnetization states. In addition, the low power consumption and the nonvolatile lateral MA states further bring alternative functionalities to the magnetoelectric devices when they are integrated together, such as switchable spin-current filtering or programmable spin-logic circuits. Moreover, by controlling the competition between interface coupling and the substrate-induced strains, it is possible to achieve the noncollinear magnetization within a continuous magnetic layer. This nontrivial artificial spin texture is significantly important for fundamental research, and also brings promising applications in orthogonal spin-transfer devices and spin oscillators [31,46].

#### IV. CONCLUSION

In summary, high-quality  $\text{SCO}_{2.5}/\text{LSMO}$  bilayer films are epitaxially grown on (110)-LSAT substrates by PLD. We find the magnetic easy axis of the LSMO layer is rotated by  $90^\circ$  in the film plane due to the interface coupling with  $\text{SCO}_{2.5}$ , from the [001] direction of the LSMO single layer to the [1̄10] direction of the  $\text{SCO}_{2.5}/\text{LSMO}$  bilayer. Interestingly, ILG causes reversible and bidirectional tuning to the strength and orientation of MA of  $\text{SCO}_{2.5}/\text{LSMO}$  bilayers. When the gating time is short, the MA constant increases or decreases, corresponding to the independent incorporation of  $\text{H}^+$  or  $\text{O}^{2-}$  ions in the  $\text{SCO}_{2.5}$  cap layer. However, when the gating time is appropriately long, the easy axis of the LSMO film reversibly switches between [1̄10] and [001] directions, corresponding to the change of electric polarity. Based on XLD analysis, it is

confirmed that the electrical controlling of Mn 3d orbital occupancy by ILG is the proximate cause for the MA switching. The preferentially occupied Mn 3d orbital is  $d_{x^2-y^2}$  for  $\text{SCO}_{2.5}/\text{LSMO}$  and  $d_{3z^2-r^2}$  for  $\text{SCO}_{3-\delta}/\text{LSMO}$ . The phase structure of  $\text{SCO}_x$  affects the relative orbital level of Mn 3d electrons. This work demonstrates the first indirect tuning to the magnetic easy axis of LSMO, providing guidance for the construction of electrically tunable magnetoelectric devices. The nonvolatility of switched MA states in the bilayer structure is a significant development for the electric modulation of magnetic devices, which demonstrates promising applications in switchable spin-current filtering or programmable spin-logic circuits.

#### ACKNOWLEDGMENTS

This work has been supported by the National Basic Research of China (Grants No. 2016YFA0300701, No. 2017YFA0206300, No. 2018YFA0305704, and No. 2017YFA0303601), the National Natural Science Foundation of China (Grants No. 11520101002, No. 51972335, No. 51590880, and No. 11674378), the Key Program of the Chinese Academy of Sciences and State Key Laboratory of Advanced Technology for Materials Synthesis and Processing (Wuhan University of Technology). We also acknowledge Beamline BL08U1A in Shanghai Synchrotron Radiation Facility (SSRF) for the XAS characterizations.

- [1] H. Y. Hwang, Y. Iwasa, M. Kawasaki, B. Keimer, N. Nagaosa, and Y. Tokura, Emergent phenomena at oxide interfaces, *Nat. Mater.* **11**, 103 (2012).
- [2] M. B. Salamon and M. Jaime, The physics of manganites: Structure and transport, *Rev. Mod. Phys.* **73**, 583 (2001).
- [3] Y. Tokura, *Gordon, Colossal Magnetoresistive Oxides* (Breach Science Publishers, Amsterdam, 2000).
- [4] Y. Tokura and Y. Tomioka, Colossal magnetoresistive manganites, *J. Magn. Magn. Mater.* **200**, 1 (1999).
- [5] Y. Q. Cai, Y. Y. Jiao, Q. Cui, J. W. Cai, Y. Li, B. S. Wang, M. T. Fernández-Díaz, M. A. McGuire, J.-Q. Yan, J. A. Alonso, and J.-G. Cheng, Giant reversible magnetocaloric effect in the pyrochlore  $\text{Er}_2\text{Mn}_2\text{O}_7$  due to a cooperative two-sublattice ferromagnetic order, *Phys. Rev. Mater.* **1**, 064408 (2017).
- [6] A. Ohtomo, D. A. Muller, J. L. Grazul, and H. Y. Hwang, Artificial charge-modulation in atomic-scale perovskite titanate superlattices, *Nature (London)* **419**, 378 (2002).
- [7] L. Y. Zhang, D. S. Xue, X. F. Xu, and A. B. Gui, Magnetic properties and Verwey transition of quasi-one-dimensional magnetite nanowire arrays assembled in alumina templates, *J. Magn. Magn. Mater.* **294**, 10 (2005).
- [8] J. Nogues and I. K. Schuller, Exchange bias, *J. Magn. Magn. Mater.* **192**, 203 (1999).
- [9] I. M. Miron, K. Garello, G. Gaudin, P. J. Zermatten, M. V. Costache, S. Auffret, S. Bandiera, R. Bernard, A. Schuhl, and P. Gambardella, Perpendicular switching of a single

- ferromagnetic layer induced by in-plane current injection, *Nature (London)* **476**, 189 (2011).
- [10] M. Weisheit, S. Fahler, A. Marty, Y. Souche, C. Poinsignon, and D. Givor, Electric field-induced modification of magnetism in thin-film ferromagnets, *Science* **315**, 349 (2007).
- [11] V. Garcia, M. Bibes, L. Bocher, S. Valencia, F. Kronast, A. Crassous, X. Moya, S. Enouz-Vedrenn, A. Gloter, D. Imhoff, C. Deranlot, N. D. Mathur, S. Fusil, K. Bouzehouane, and A. Barthélémy, Ferroelectric control of spin polarization, *Science* **327**, 1106 (2010).
- [12] C. G. Duan, J. P. Velev, R. F. Sabirianov, Z. Zhu, J. Chu, S. S. Jaswa, and E. Y. Tsymbal, Surface Magnetoelectric Effect in Ferromagnetic Metal Films, *Phys. Rev. Lett.* **101**, 137201 (2008).
- [13] K. Nakamura, R. Shimabukuro, Y. Fujiwara, T. Akiyama, T. Ito, and A. J. Freeman, Giant Modification of the Magnetocrystalline Anisotropy in Transition-Metal Monolayers by an External Electric Field, *Phys. Rev. Lett.* **102**, 187201 (2009).
- [14] M. Tsujikawa and T. Oda, Finite Electric Field Effects in the Large Perpendicular Magnetic Anisotropy Surface  $P_t = Fe = Pt(001)$ : A First-Principles Study, *Phys. Rev. Lett.* **102**, 247203 (2009).
- [15] J. Stohr, H. C. Siegmann, A. Kashuba, and S. J. Gamble, Magnetization switching without charge or spin currents, *Appl. Phys. Lett.* **94**, 072504 (2009).
- [16] N. N. Negulyaev, V. S. Stepnyuk, W. Hergert, and J. Kirschner, Electric Field as a Switching Tool for Magnetic States in Atomic-Scale Nanostructures, *Phys. Rev. Lett.* **106**, 037202 (2011).
- [17] M. McCaig, *Permanent Magnets in Theory and Practice* (Wiley, NY, 1977).
- [18] J. W. Lee, S. C. Shin, and S. K. Kim, Spin engineering of CoPd alloy films via the inverse piezoelectric effect, *Appl. Phys. Lett.* **82**, 2458 (2003).
- [19] X. Hong, J.-B. Yau, J. D. Hoffman, C. H. Ahn, Y. Bason, and L. Klein, Effect of electric field doping on the anisotropic magnetoresistance in doped manganites, *Phys. Rev. B* **74**, 174406 (2006).
- [20] H. J. A. Molegraaf, J. Hoffman, C. A. F. Vaz, S. Gariglio, D. van der Marel, C. H. Ahn, and J.-M. Triscone, Magnetoelectric effects in complex oxides with competing ground states, *Adv. Mater.* **21**, 3470 (2009).
- [21] D. Chiba, M. Sawicki, Y. Nishitani, Y. Nakatani, F. Matsukura, and H. Ohno, Magnetization vector manipulation by electric fields, *Nature (London)* **455**, 515 (2008).
- [22] B. Cui, C. Song, G. A. Gehring, F. Li, G. Wang, C. Chen, J. Peng, H. Mao, F. Zeng, and F. Pan, Electrical manipulation of orbital occupancy and magnetic anisotropy in manganites, *Adv. Func. Mater.* **25**, 864 (2015).
- [23] H. Y. Hwang, S.W. Cheong, N. P. Ong, and B. Batlogg, Spin-Polarized Intergrain Tunneling in  $\text{La}_{2/3}\text{Sr}_{1/3}\text{MnO}_3$ , *Phys. Rev. Lett.* **77**, 2041 (1996).
- [24] Y. Suzuki, H. Y. Hwang, S. W. Cheong, T. Siegrist, R. B. van Dover, A. Asamitsu, and Y. Tokura, Magnetic anisotropy of doped manganite thin films and crystals, *J. Appl. Phys.* **83**, 7064 (1998).
- [25] C. Tannous and J. Gieraltowski, The Stoner-Wohlfarth model of ferromagnetism, *Eur. J. Phys.* **29**, 475 (2008).
- [26] L. M. Berndt, V. Balbarin, and Y. Suzuki, Magnetic anisotropy and strain states of (001) and (110) colossal magnetoresistance thin films, *Appl. Phys. Lett.* **77**, 2903 (2000).
- [27] P. Bruno, Tight-binding approach to the orbital magnetic moment and magnetocrystalline anisotropy of transition-metal monolayers, *Phys. Rev. B* **39**, 865 (1989).
- [28] P. Bruno, *Magnetismus Von Festkörpern und Grenzflächen, Ferienkurse des Forschungszentrums Jülich* (KFA, Jülich, Germany, 1993), Chap. 24, p. 1.
- [29] D. Pesquera, G. Herranz, A. Barla, E. Pellegrin, F. Bondino, E. Magnano, F. Sanchez, and J. Fontcuberta, Surface symmetry-breaking and strain effects on orbital occupancy in transition metal perovskite epitaxial films, *Nat. Commun.* **3**, 1189 (2012).
- [30] Z. Liao, M. Huijben, Z. Zhong, N. Gauquelin, S. Macke, R. J. Green, S. van Aert, J. Verbeeck, G. van Tendeloo, K. Held, G. A. Sawatzky, G. Koster, and G. Rijnders, Controlled lateral anisotropy in correlated manganite heterostructures by interface-engineered oxygen octahedral coupling, *Nat. Mater.* **15**, 425 (2016).
- [31] D. Yia, J. Liu, S. L. Hsu, L. Zhang, Y. Choi, J. W. Kim, Z. Chen, J. D. Clarkson, C. R. Serra, E. Arenholz, P. J. Ryan, H. Xu, R. J. Birgeneau, and R. Rames, Atomic-scale control of magnetic anisotropy via novel spin-orbit coupling effect in  $\text{La}_{2/3}\text{Sr}_{1/3}\text{MnO}_3/\text{SrIrO}_3$  superlattices, *PNAS* **113**, 6397 (2016).
- [32] J. Zhang, Z. Zhong, X. Guan, X. Shen, J. Zhang, F. Han, H. Zhang, H. Zhang, X. Yan, Q. Zhang, L. Gu, F. Hu, R. Yu, B. Shen, and J. Sun, Symmetry mismatch-driven perpendicular magnetic anisotropy for perovskite/brownmillerite heterostructures, *Nat. Commun.* **9**, 1923 (2018).
- [33] H. Jeen, W. S. Choi, J. W. Freeland, H. Ohta, C. U. Jung, and H. N. Lee, Topotactic phase transformation of the brownmillerite  $\text{SrCoO}_{3-\delta}$  to the perovskite , *Adv. Mater.* **25**, 3651 (2013).
- [34] H. Jeen, W. S. Choi, M. D. Biegalski, C. M. Folkman, I. C. Tung, D. D. Fong, J. W. Freeland, D. Shin, H. Ohta, M. F. Chisholm, and H. N. Lee, Reversible redox reactions in an epitaxially stabilized  $\text{SrCoO}_x$  oxygen sponge, *Nat. Mater.* **12**, 1057 (2013).
- [35] L. Karvonen, M. Valkeap, R. S. Liu, J. M. Chen, H. Yamauchi, and M. Karppine, O-K and Co-L XANES study on oxygen intercalation in perovskite  $\text{SrCoO}_{3-\delta}$  , *Chem. Mater.* **22**, 70 (2010).
- [36] N. Lu, et al., Electric-field control of tri-state phase transformation with a selective dual-ion switch, *Nature (London)* **546**, 124 (2017).
- [37] See Supplemental Material at <http://link.aps.org/supplemental/10.1103/PhysRevApplied.12.054016> for experimental details.
- [38] J. Song, Y. Chen, H. Zhang, F. Han, J. Zhang, X. Chen, H. Huang, J. Zhang, H. Zhang, X. Yan, T. Khan, S. Qi, Z. Yang, F. Hu, B. Shen, and J. Sun, Strong anisotropy and its electric tuning for brownmillerite  $\text{SrCoO}_{2.5}$  films with different crystal orientations, *Phys. Rev. Mater.* **3**, 045801 (2019).
- [39] M. Martin, G. Shirane, Y. Endoh, K. Hirota, Y. Moritomo, and Y. Tokura, Magnetism and structural distortion

- in the  $\text{La}_{0.7}\text{Sr}_{0.3}\text{MnO}_3$  metallic ferromagnet, *Phys. Rev. B* **53**, 14285 (1996).
- [40] A. Munoz, C. de la Calle, J. A. Alonso, P. M. Botta, V. Pardo, D. Baldomir, and J. Rivas, Crystallographic and magnetic structure of  $\text{SrCoO}_{2.5}$  brownmillerite: Neutron study coupled with band-structure calculations, *Phys. Rev. B* **78**, 054404 (2008).
- [41] H. Boschker, M. Mathews, P. Brinks, E. Houwman, A. Vailionis, G. Koster, D. Blank, and G. Rijnders, Uniaxial contribution to the magnetic anisotropy of  $\text{La}_{0.67}\text{Sr}_{0.33}\text{MnO}_3$  thin films induced by orthorhombic crystal structure, *J. Magn. Magn. Mater.* **323**, 2632 (2011).
- [42] V. Bhosle and J. Narayan, Epitaxial growth and magnetic properties of  $\text{La}_{0.7}\text{Sr}_{0.3}\text{MnO}_3$  films on (0001) sapphire, *Appl. Phys. Lett.* **90**, 101903 (2007).
- [43] V. Bhosle, J. T. Prater, and J. Narayan, Anisotropic magnetic properties in [110] oriented epitaxial  $\text{La}_{0.7}\text{Sr}_{0.3}\text{MnO}_3$  films on (0001) sapphire, *J. Appl. Phys.* **102**, 013527 (2007).
- [44] Y. Tsujimoto, C. Tassel, N. Hayashi, T. Watanabe, H. Kageyama, K. Yoshimura, M. Takano, M. Ceretti, C. Ritter, and W. Paulus, Infinite-layer iron oxide with a square-planar coordination, *Nature (London)* **450**, 1062 (2007).
- [45] Y. Zhou, X. Guan, H. Zhou, K. Ramadoss, S. Adam, H. Liu, S. Lee, J. Shi, M. Tsuchiya, D. D. Fong, and S. Ramanathan, Strongly correlated perovskite fuel cells, *Nature (London)* **534**, 231 (2016).
- [46] A. Brataasa, G. E. W. Bauer, and P. J. Kelly, Non-collinear magnetoelectronics, *Phys. Rep.* **427**, 157 (2006).